Draft report

Innovative Design for a Rapidly Deployable Shelter

Written 17/12/2007

Jonathan TAYLOR MEng,

Research Assistant, Department of Engineering Science, University of Oxford, Oxford, OX1 3PJ

E-mail: jont.mail@gmail.com

Zhong YOU BSc PhD

University Lecturer (Structures), Department of Engineering Science, University of Oxford, OX1 3PJ

Telephone: +44 (0)1865 2 73137, Fax: +44 (0)1865 2 83301, E-mail: zhong.you@eng.ox.ac.uk

Number of Words: *3062*

Number of Figures: *13*

Number of Tables: *2*

Key Words: *Mathematical modelling, Models (physical), Structural frameworks*

Abstract: *157 words*

Humanitarian crises and warfare require large shelters capable of housing displaced people, for emergency remote hospitals and for military equipment. Existing designs for large span shelters are scalable and versatile, but are often not utilised because of the time and efforts required for transport and deployment. This paper investigates the use of tiling Bennett linkages to construct a large span arch, which addresses these issues. The geometry of the Bennett linkage, a 4R linkage, is analysed and constituent equations are composed. Constraints are determined to enable a network of Bennett linkages to form a folding tunnel. The hinge design for the linkage is modelled and tested using Finite Element Analysis (FEA). A prototype arch is designed, built and tested to validate the FEA. A good correlation is found between the physical testing of the prototype and the computational modelling. The FEA is shown to be useful in modelling the arch in a number of modes of loading.

Notation:

α, β: Angle of twist from one revolute axis to the next (rad)

γ: Opening angle of a Bennett linkage in 3-dimensions (rad)

θ: Opening angle between two bars in a linkage (rad)

The Bennett Linkage

Escalating frequency of humanitarian crises and warfare around the world have highlighted a huge demand for large shelters capable of housing displaced people, providing shelter from the weather, for emergency remote hospitals and for military equipment. Large shelters must be capable of air-lifting into disaster areas and be assembled and deployed rapidly by relatively few people. Conflicts in the Arabian Gulf, Afghanistan and Iraq required the use of a rapidly deployable large span shelter to protect and camouflage forward attack helicopters. Existing designs are scalable and modular and so their use is versatile, but the time and effort required to transport and deploy the structures means that they do not always get used[1].

Commonplace tent and shelter designs use many techniques; rigid trusses and fabric covers, inflatable columns and beams, flexible struts, guy ropes and interlocking rigid beams to achieve a both a large volume within a covered frame and disassembled configurations. Existing deployable structures[2] require assembly prior to deployment adding to the time burden.

The Bennett linkage is a four-bar revolute joint based (4R) mechanism developed early in the 20th Century[3]. The Bennett linkage provides a unique deployable mechanism, which could be used to construct the frame of a large span shelter. The mechanism uses only rigid structural elements connected with revolute joints and can be scaled and repeated to almost any required size required. The Bennett mechanism is capable of allowing frame

to pack into a compact bundle for storage or transport, solving issues with existing large span shelters

Figure 1 shows the basic Bennett linkage ABCD. The diagram shows the nodes at A, B, C and D, the directions of the revolute axis at each node and the constituent angles θ and α. θ_{M} is the instantaneous angle between the two bars of the linkage at node M. α_{MN} is the angle of twist between the revolute axes from node M to N. Revolute axes are perpendicular to both bars the revolute axis intersects; the twist α is measured about the axis of the bar.

Compatibility equations for the linkage are developed in full by Chen[4] and Beggs[5]; Alternate sides ($\overline{\mathrm{AB}}$, etc.) of the loop have the same length (a, etc.) and twist angles,

$$\overline{\mathrm{AB}} = \overline{\mathrm{CD}} = a \tag{1}$$
$$\overline{\mathrm{BC}} = \overline{\mathrm{DA}} = b \tag{2}$$
$$\alpha_{\mathrm{AB}} = \alpha_{\mathrm{CD}} = \alpha \tag{3}$$
$$\alpha_{\mathrm{BC}} = \alpha_{\mathrm{DA}} = \beta \tag{4}$$

The lengths and twists satisfy the condition

$$\frac{\sin\alpha}{a} = \frac{\sin\beta}{b} \tag{5}$$

The revolute variables θ_{M}, θ_{N}, etc. are dependent on the opening of the linkage. The three closure equations are provided by the relations in Equations 6 to 8.

$$\theta_{\mathrm{A}} + \theta_{\mathrm{C}} = 2\pi \tag{6}$$
$$\theta_{\mathrm{B}} + \theta_{\mathrm{D}} = 2\pi \tag{7}$$

$$\tan\frac{\theta_A}{2}\tan\frac{\theta_B}{2}=\frac{\sin\frac{1}{2}(\beta+\alpha)}{\sin\frac{1}{2}(\beta-\alpha)} \tag{8}$$

Equations 6 to 8 reduce the compatibility conditions to a single degree of freedom and hence, the linkage has mobility of one[6]. When the linkage is viewed in three dimensions (Figure 2) the loop ABCD shows that the linkage bends through an angle γ, as it is deployed.

Geometric analysis of the equilateral form of the linkage can be performed using geometry of the tetrahedral shape in Figure 2, where M is the mid-point of BD and N is the mid-point of AC. The equations thus derived are reduced to provide the useful result of the bend angle in terms of deployment angles[2].

$$\cos\gamma=1-2\frac{1+\cos\theta_B}{1-\cos\theta_A} \tag{9}$$

As the linkage is equilateral $a=b$, hence $\alpha=\pi-\beta$ satisfies Equation 3. The third loop closure condition (Equation 8) becomes

$$\tan\frac{\theta_A}{2}\tan\frac{\theta_B}{2}=\frac{1}{\cos\alpha} \tag{10}$$

Tiling of the Linkages

Figure 3 shows one tiling of overlapping and connected Bennett linkages. ‘Child’ 4-bar loops are created by the tiling of the larger ‘parent’ 4-bar loops. For the tiled linkages to work as a mechanism, all of the child 4-bar loops numbered 1-8 must be valid Bennett

linkages in their own right. The ratio of lengths $\overline{AB}$ to $\overline{BC}$ determines the shape of the deployed network. If $\overline{AB}$ and $\overline{BC}$ are unequal the network will form a helical shape, if $\overline{AB}$ and $\overline{BC}$ are equal the network will take on a cylindrical shape. The networks theoretically fold from one extreme to the other. Fully compacted to one limit, the radius of the helix tends to infinity and network forms a long straight line of coincident links, beyond the shape shown in Figure 4 (i). The network then deploys into a helix as in Figure 4 (ii). If deployed beyond this to the limit, the shape becomes compacted into a line perpendicular to the previous compacted axis as the radius tends to zero, shown in Figure 4 (iii). This project makes use of the cylindrical form of the linkage.

This project aims to develop the cylindrical form of the Bennett linkage based network into a functional shelter. This requires developing a finite element based computational tool to design and to predict behaviour of a Bennett linkage frame then to build and test a large model frame to validate or modify this computational method. Figure 5 shows a Bennett link based arch designed by Yan Chen[4]. This frame could be tiled to create a larger tiled Bennett network and contains visible redundant bars. A similar frame will be modelled and constructed to test the concept. Firstly the full geometry of a Bennett link based arch is developed.

Geometric Construction

When the cylindrical network is deployed and viewed from the side, the network forms a cylinder or an arch. The arch is then deployed so that the sides at either end of the arch

are parallel. When viewed from the side, the open arch forms part of the shape of a regular polygon, which is continued beyond the base of the arch. The geometry of the polygon provides enough equations that once the designer has determined the required height and span of the frame, the opening angle when deployed and the maximum length dimension when compacted, the rest of the geometry can be calculated. The necessary calculations do not require iteration or user input to produce a valid Bennett linkage frame, which will cover any desired plan area. The dimensions of the structural bars can also be input and will determine the complete compacted dimensions of the frame.

Physical Construction

The frame in Figure 5 was constructed by drilling holes through carbon fire composite tubes and fitting aluminium bars through the holes to form simple pin joints. The central planes in which the revolute axes are arranged are located in between the planes containing the tubes. The revolute axes are aligned along the central axis of the tube, not aligned along the edge of the tube in contact with the central plane. The model frame operates as a mechanism because of the play present in the hinge bars; a fully rigid structure constructed like this would fail to work as a mechanism. A new type of hinge mechanism must be designed to allow the revolute axes to be positioned in the correct plane. By interrupting the line of the bars a revolute hinge can be inserted in the correct position and alignment. Such a hinge is seen in Figure 6, showing how the hinge stops in the deployed position and fully compacts into a cylindrical section. The central plane of

each of these hinges contains a point where the revolute axis crosses the construction plane.

A final large scale prototype was constructed using this type of hinge. The hinges were machined from Nylon-6 and joined with carbon fibre reinforced composite tubes. Araldite 2011 Epoxy was used to join the tubes to the hinges and needle roller bearings allow smooth rotation at the hinges. For an arch to span 8 m and a height of 5 m a total weight of around 52 kg was calculated. Further details are given in Table 1.

Finite Element Model Construction

A geometric construction methodology was built in numerical computing application using the equations summarised earlier. A beam element based finite element model was written to a text based input file. The text file contained the frame geometry, beam types, cross-section dimensions and material data for both the composite tubes and nylon hinges. The directions for the revolute hinges are defined and the model has the ability to tie the hinges in position when deployed or to allow rotation. The boundary conditions at the ground connection are initially pinned and constrained to only allow rotation in one direction to represent the way the aluminium feet are restrained by T-shaped ground plates anchored to the ground. The slight zigzag in the geometry in each length of bar now present is modelled by alternating long composite and short nylon elements as can be seen in that arch shown in Figure 7. Self-weight for the tubes was calculated and

applied by Abaqus but self-weight for the hinges was measured from the final weight for a hinge pair with all necessary fittings then applied as point loads.

Some simple load tests were run on the finite element arch to predict behaviour of the prototype arch. It was necessary to allow for nonlinear geometric effects; displacements and rotations of the elements in the frame could be quite large. Two modes of loading were applied to the frame; a load applied down equally at the two nodes at the top of the frame and a single load acting sideways from one of the top nodes. The data from these tests was first used to check the performance of the beam elements used to approximate the hinges in the finite element frame and to estimate magnitudes of displacement of the prototype.

Once the prototype frame had been constructed an extra modification to the FEA generating code had to be added. Due to the geometry of rotating the hinge pieces about the tube axis instead of the imaginary Bennett link axis, the hinges on the outside edges of the frame did not line up well enough to allow the hinges to be locked. The arc the hinge centre travels through is something to careful of when redesigning the hinge. An earlier prototype with more slender bars and less stiff bonding of the hinges failed to reveal this effect as the arcs were mush less significant.

Finite Element Hinge Modelling

The CAD files used to produce the hinge parts were slightly simplified and imported into the Abaqus. From there the model was meshed and loaded. The tests on the beam element model arch provided data including section forces and moments for each element and the graphical interface can be used to identify the most stressed element. The forces and moments can then be extracted from the output files and then applied to the connecting lugs of the solid element model hinge to accurately represent the forces transferred by the hinge. Boundary conditions must be sufficient to restrain the motion of the hinge accurately. Depending on how the hinge was being loaded, different faces and partitions were restricted in the relevant degrees of freedom, as if they were in contact with a similar face or the partition is restrained by a bolt. This required that sometimes two simulations were run for each loading investigated but provided much better performance and resolution than a full contact simulation.

This technique was used to examine the hinge stress for an arch undergoing a vertical load test at the two points at the arch centre. Figure 8 shows that the beam model predicts stress behaviour reasonably close to that found with the solid element modelling. The beam model stresses were higher than determined by the solid modelling and not always in the same location suggested by the beam model. This suggests that some redesign of the hinge element type is needed to accurately predict failure of the elements. The Ultimate Tensile Stress provided by the manufacturer suggests that the hinges will undergo plastic failure when the arch is loaded above 175 N.

Erecting the Arch and Deformation Under Self-Load

Erecting the frame required tree people – two to lift the frame by hand, then once lifted some way off the ground, the third with a strong pole, to push the top of the frame up and forward with the first two providing additional support and control.

Once erected, the deformed shape under self-load was measured and compared to the expected shape. Measurements of key points were compared, notably, the distance between the hinges anchored to the ground, the distance between the hinges initially one side (about 1.8 m) above these, and the distance from the top hinges down to ground level. Table 2 summarises the undeformed and deformed distances predicted by FEA and recorded form the prototype. The prototype arch is flexible enough that the neutral, unstressed shape was difficult to find on rough ground. When pulled to the same shape as designed, the dimensions of the arch matched the design shape well. When erected and deforming under its own weight, the arch sunk at the top and bowed out at the sides as expected.

Simple Loading of the Arch

After assembling the arch simple tests were first run on the prototype arch. Loads were applied in 0.5 kg increments up to 6 kg, in addition to an initial load from the hanging weight platform; 2.43 kg. A light rope was hitched to the opposite hinges at the top, from which the weights could be suspended from. A steel tape measure was bolted securely to one of these top nodes to provide a measurement distance.

A chart summarising these measurements can be found in Figure 9, comparing the FE modelled response to vertical loading with the measured response from the prototype arch, which is an average of 3 incremental load cases. As can be seen, a linear region of response was recorded however the linear stiffness was over 2.75 times greater than predicted, 936 N/m vs. 340 N/m. A match for the linear region could be found by increasing the stiffness of the nylon joints by a factor of 2.8 and by making the ground connections flexible to mimic the flexure of the ground plates. Matches for the deformation under self-load and under additional load could not be produced concurrently; there was significant amount initial sag before the ground connections are fixed securely.

Side Loading of the Arch

Testing of the arch under a side-load was conducted by securing a strap around one of the nodes towards the top of the arch, and pulling the node towards a point on the ground a reasonable distance away. The strap was shortened with a cam buckle to load the frame and a pair of spring balances in parallel allowed measurement of the load up to 20 kg. The prototype arch did not displace as much as expected vertically but displaced more horizontally under a given load; a different mode of behaviour was being recorded than was predicted by the FEA. Figure 10 shows how the mode of deformation of the prototype arch compares with the original FE model and a FE model with modified stiffness. To achieve this match, the stiffness of the hinge elements was increased 6-fold

and the stiffness of the ground elements reduced to 1/10 of the stiffness of the round profile aluminium fixings. Observation tallies this flexibility with the T-shaped ground plates bowing into the ground under load and not the aluminium ends bending. The load-displacement plot is shown in Figure 11, where it is shown that the vertical displacements and near-side rotations match well. The far side rotation (RHS) is not as accurate but could be due to ground conditions varying or nonlinear behaviour of the ground connections.

Asymmetric Testing of the Arch

A vertical load was applied to the arch at the same node as the side pull test, approximately half way from the centre of the arch to the side, by means of a hanging weight. Vertical deformation was measured at the central node as before. An incline gauge was taped to the one side of the arch and the angle read off the gauge. As there was only one gauge, fewer measurements were made for this rotation than the central deflection and hence there is more scatter in these results and the experiment was repeated several times at a different location another day to find another data set. A modified stiffness model could be made to fit the central deflection and LHS slope profiles adequately. Figure 12 shows the results of this model plotted against the experimental results; the large difference seen with the RHS slope was aggravated by the difficulty taking accurate readings of the slope and could be caused by the effective stiffness of the ground increasing as the side falls over. Again, the effective stiffness of

the nylon hinges is increased, this time by a factor of 3.25 above the initial stiffness, to achieve this match.

Addition of Bracing to the Arch

Further tests were carried out with the addition of a pair of rigid braces to the prototype arch. Once the prototype arch had been expanded on the ground, a thin bar was bolted horizontally across the open diamond, about 1.8 m from base level. The arch is then erected as normal. The bar restrained the motion of these nodes, increasing the initial sag stiffness of the arch and decreasing the linear stiffness by a small amount as shown in Figure 13. The FEA predicted a small 20 mm reduction in central deflection with the addition of bracing, where in the prototype arch a larger 56 mm reduction was experienced. This increase in initial stiffness is due to the fact that the hinges when close to vertical have very little rotational stiffness due to the small amount of play in the mounting lugs. The decrease in linear stiffness could be because the ground connections are providing less stiffness than when in full contact.

Comparison of FEA to Prototype

The FEA modelling has shown that the effective stiffness of the hinge is consistently higher than the simple model used in the FE beam modelling. As the stiffness experienced is different depending on the mode of loading, a different hinge element profile is required to better model the nylon hinge.

The adjustment factors for the stiffnesses and testing have shown themselves to be reproducible for the prototype arch. The existing finite element modelling code is a useful tool in the design of similar arches, but to ensure maximum suitability for further design, modifications must made to represent the findings of the prototype testing.

The prototype arch seen has been shown to be a useful building element for an advanced, lightweight and adaptable shelter. Further modelling using the code written can design a full scale shelter capable of withstanding wind and snow loads required.

References

[1] Melin, N O (2004) *Application of Bennett Mechanisms to Long-Span Shelters.* DPhil Thesis, University of Oxford.

[2] http://www.tentnology.com/sites/default/files/pdf/ss_specs.pdf

[3] Bennett, G T (1903), *A new mechanism*, Engineering, 76, 777-778.

[4] Chen, Y (2003) *Design of Structural Mechanisms*. DPhil Thesis, University of Oxford.

[5] Beggs, J S (1966), *Advanced Mechanism*, Macmillan Company, New York.

[6] Baker, E J (1979), *The Bennett, Goldberg and Myard linkages – in Perspective*, Mechanism and Machine Theory, 14, 239-253.

Table 1 – Specification of prototype arch

Parameter	Specification	
Shelter width	W	8.00 m
Shelter height	H	5.01 m
Twist angle	α	29.19°
Number of polygon sides	n	14
Bend in Bennett link	γ	154.3°
Bar outside radius	r	26 mm
Bar thickness	t	3mm
Bar length (node-to-node)	l	1 m
Number of bars in arch	32	
Number of hinges in arch (including ground)	26	
Mass of one CFRP bar	0.465 kg	
Mass of one nylon hinge pair inc. metalwork	1.465 kg	
Predicted mass of prototype arch	52.97 kg	
Measured mass of prototype arch	49 kg	

Table 2 – Comparison of distances predicted and recorded from prototype arch under self-load

FEA model	Undeformed distance (m)	Deformed distance under self-load (m)
Width at base	8.00	8.00
Width above base	8.00	8.22
Height	5.01	4.65
Prototype	**Undeformed distance (m)**	**Deformed distance under self-load (m)**
Width at base	8.00	8.02
Width above base	8.00	8.25
Height	5.05	4.75

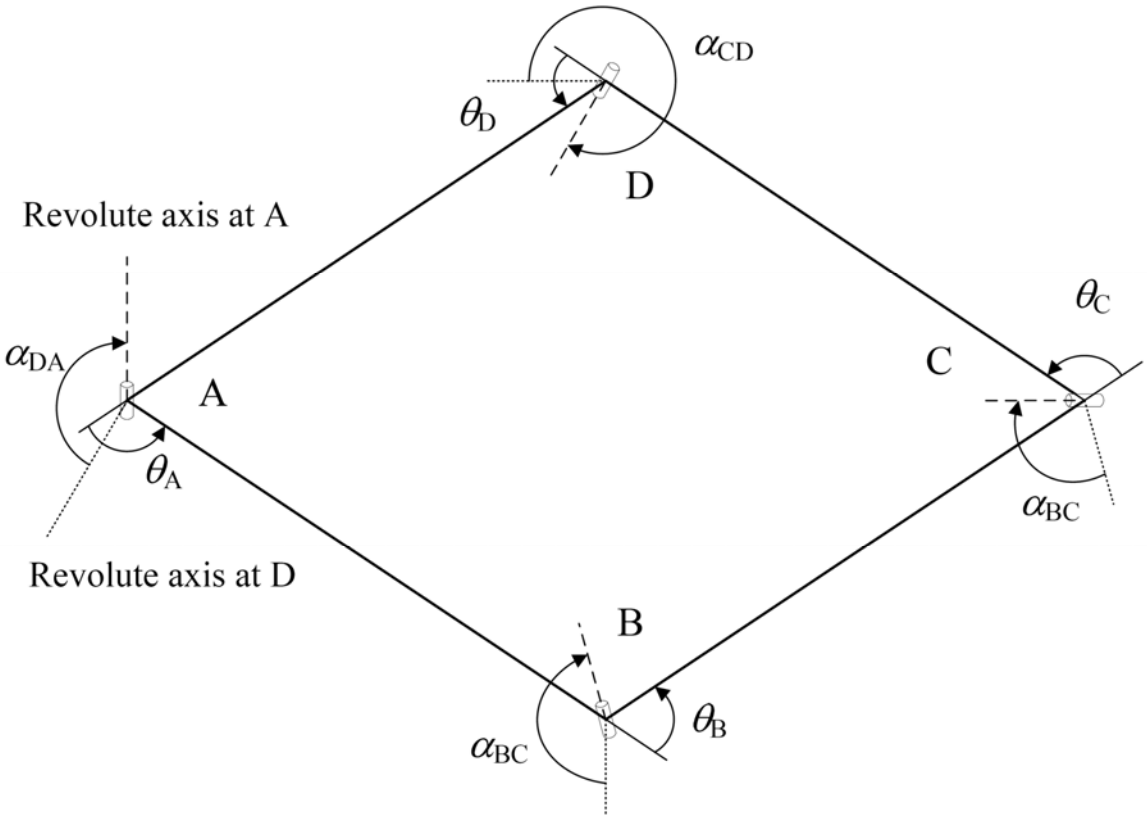

Figure 1 – A Bennett mechanism

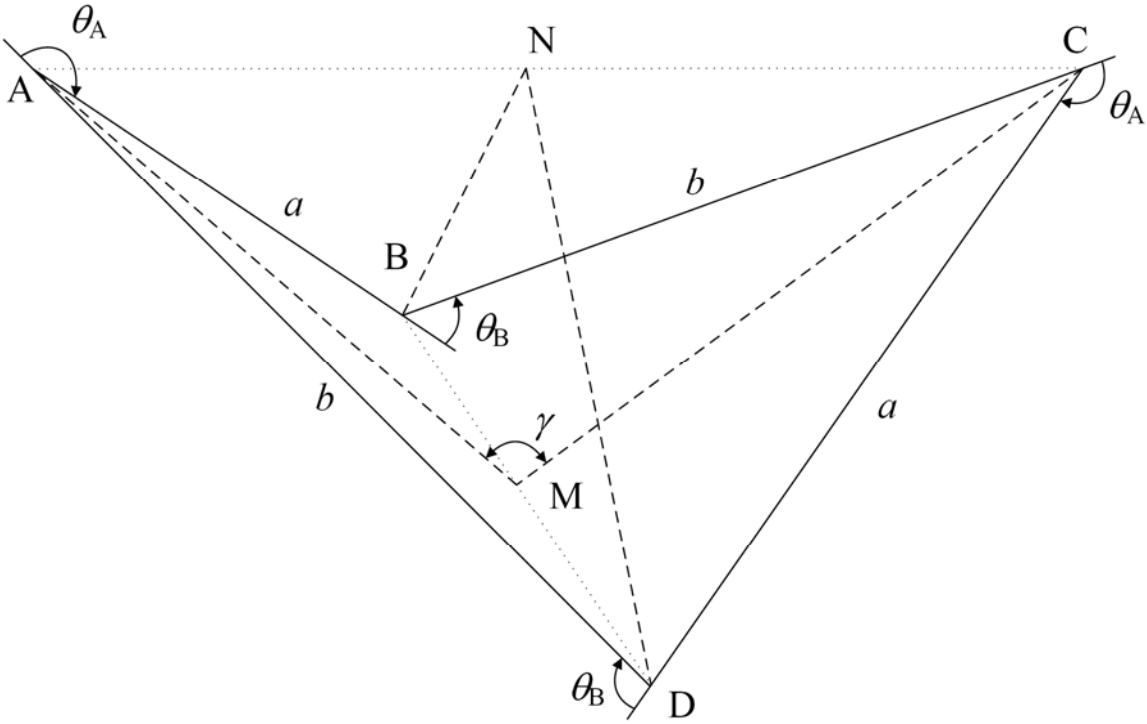

Figure 2 – 3D view of a deformed equilateral Bennett linkage with bend γ between the two planes

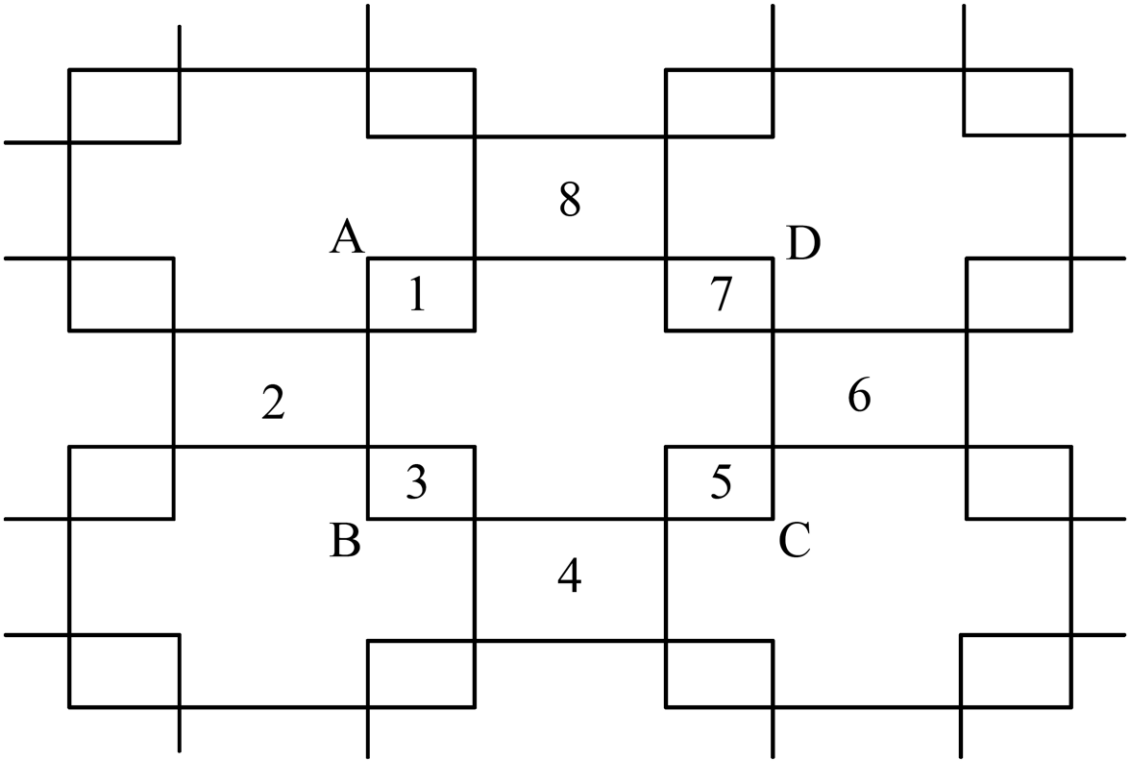

Figure 3 – A network of Bennett linkages

Figure 4 – A network of Bennett linkages (i) compacted as R $\rightarrow$ infinity, (ii) mid-deployment, (iii) compacted into a cylinder as R $\rightarrow$ 0

Figure 5 – The early prototype Bennett arch[4]

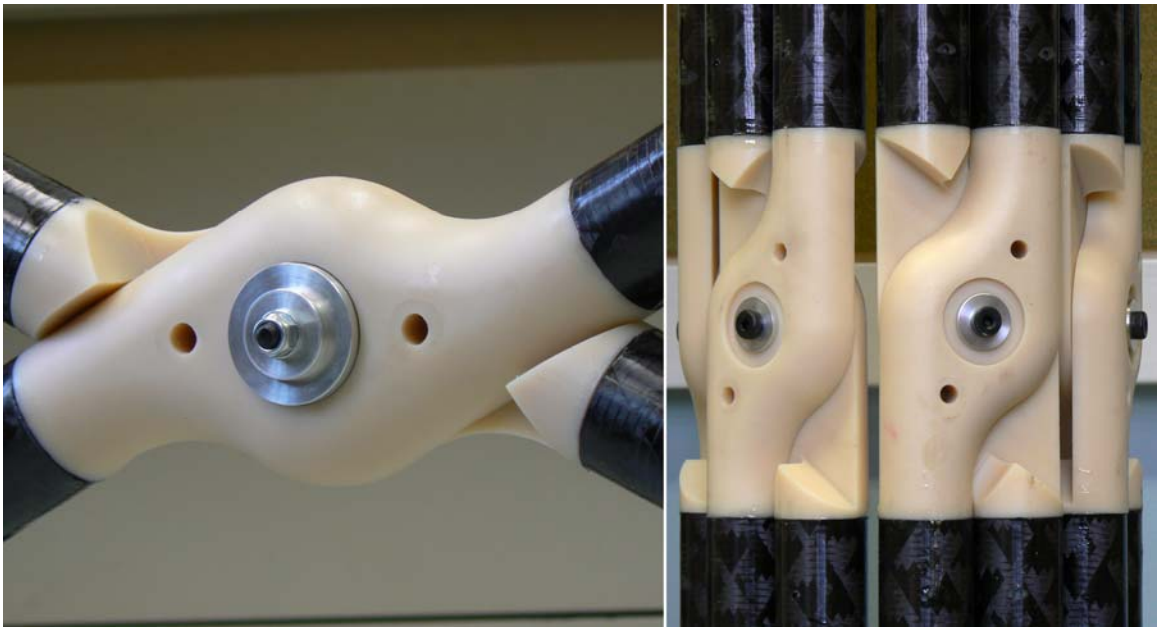

Figure 6 –The production hinge when deployed and when compacted

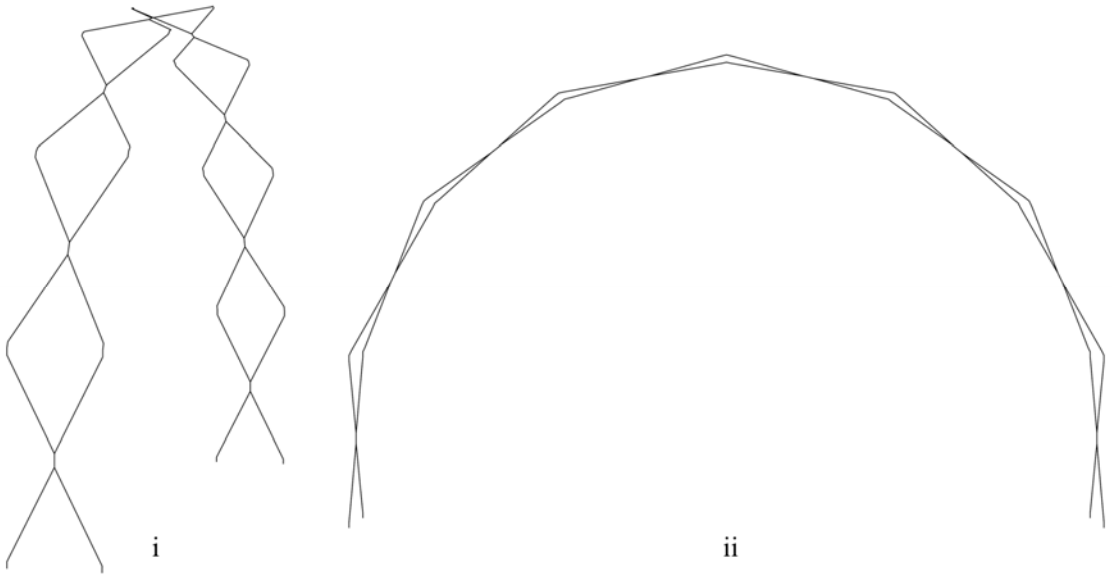

Figure 7 – Finite element model of the prototype folding arch: (i) isometric view, (ii) side view

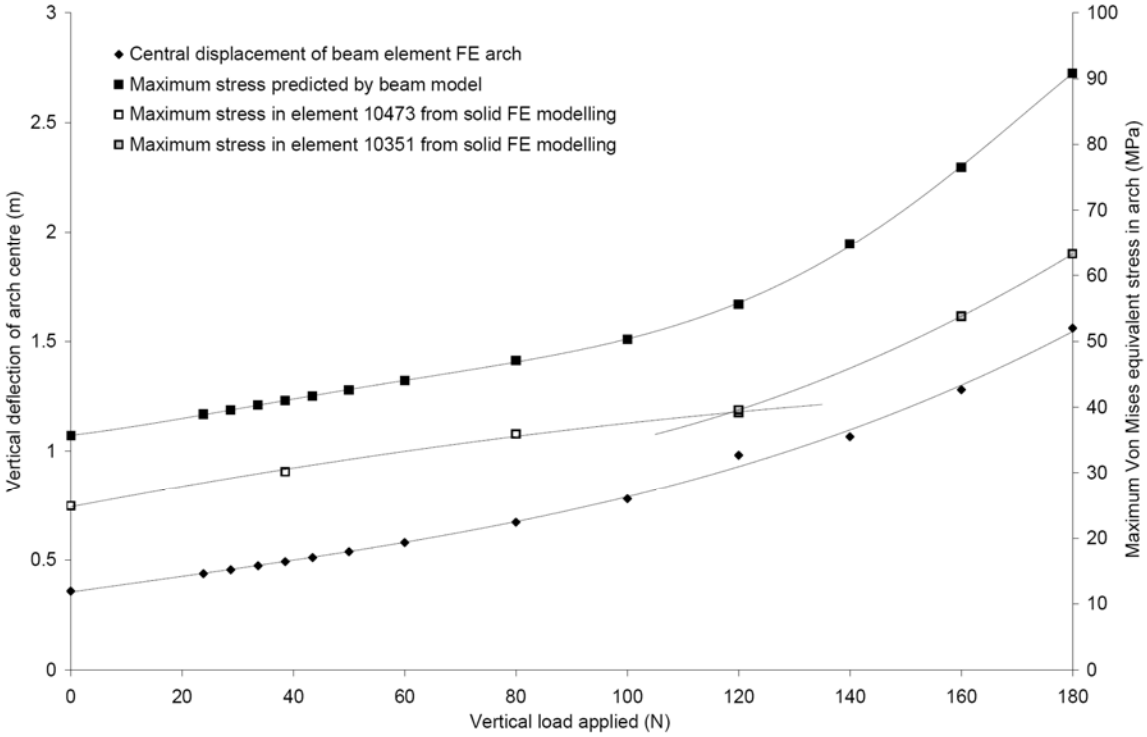

Figure 8 – Comparison of finite element Bennett arch beam element model with solid element hinge modelling

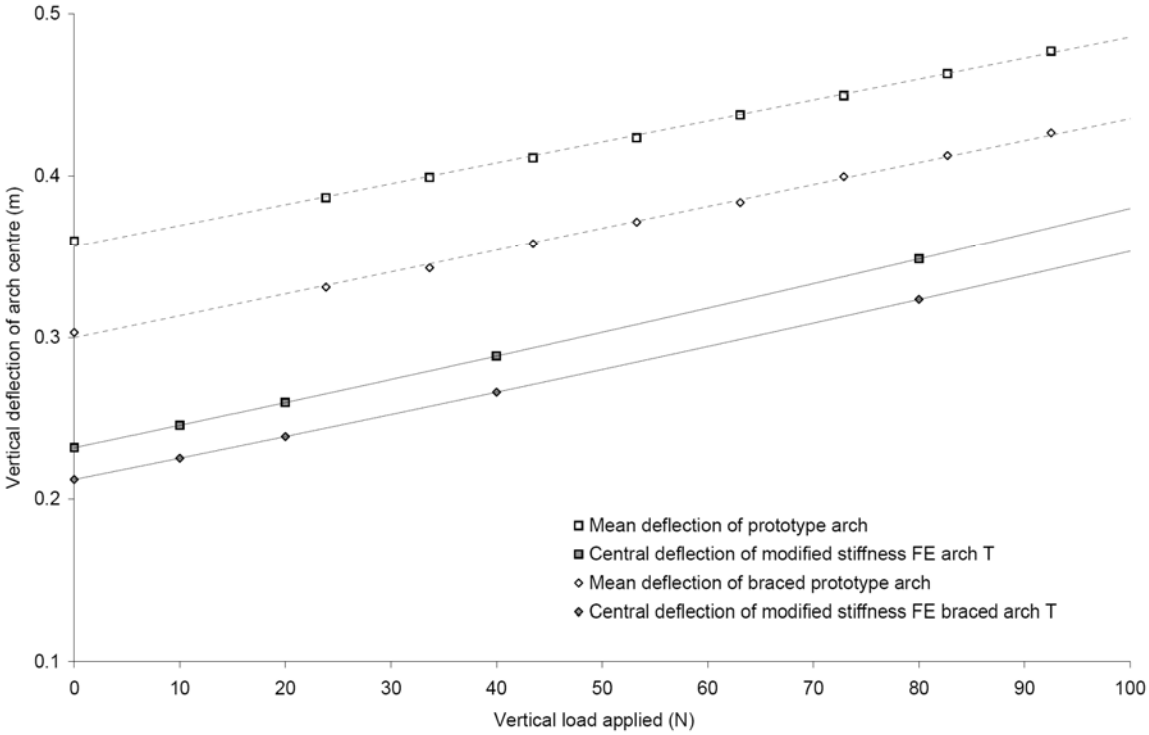

Figure 9 – Comparison of FEA model with prototype arch under central load tests

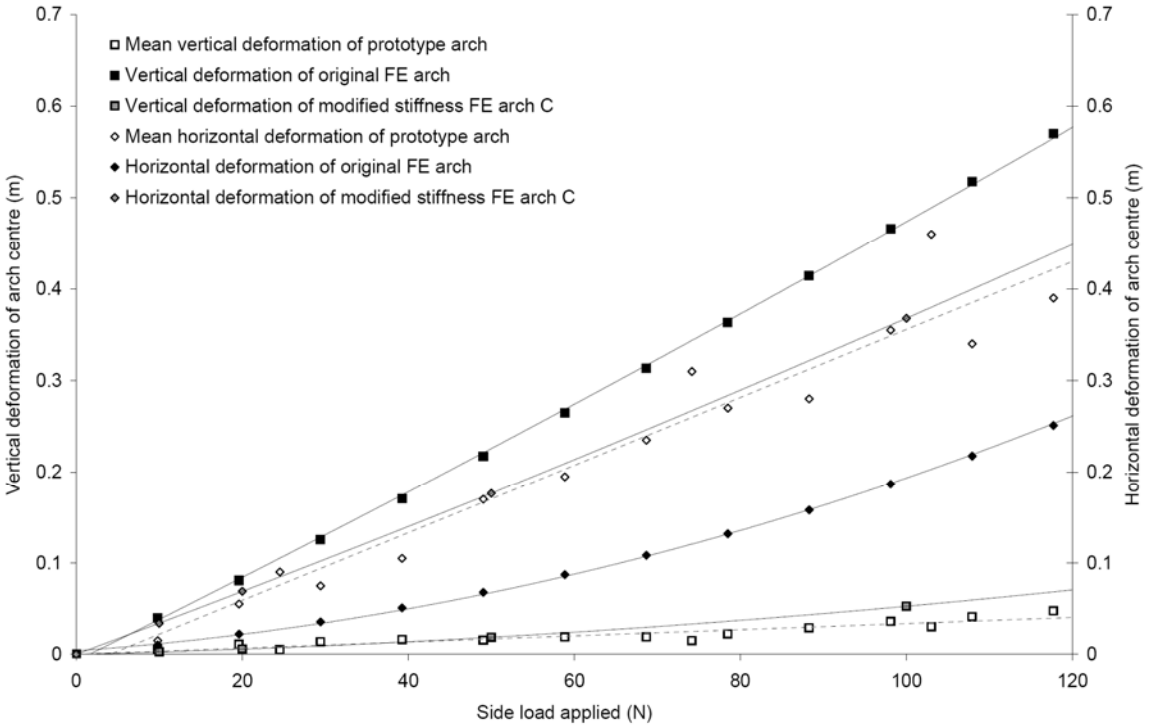

Figure 10 – Modes of deformation of finite element models and prototype arch under side-load tests

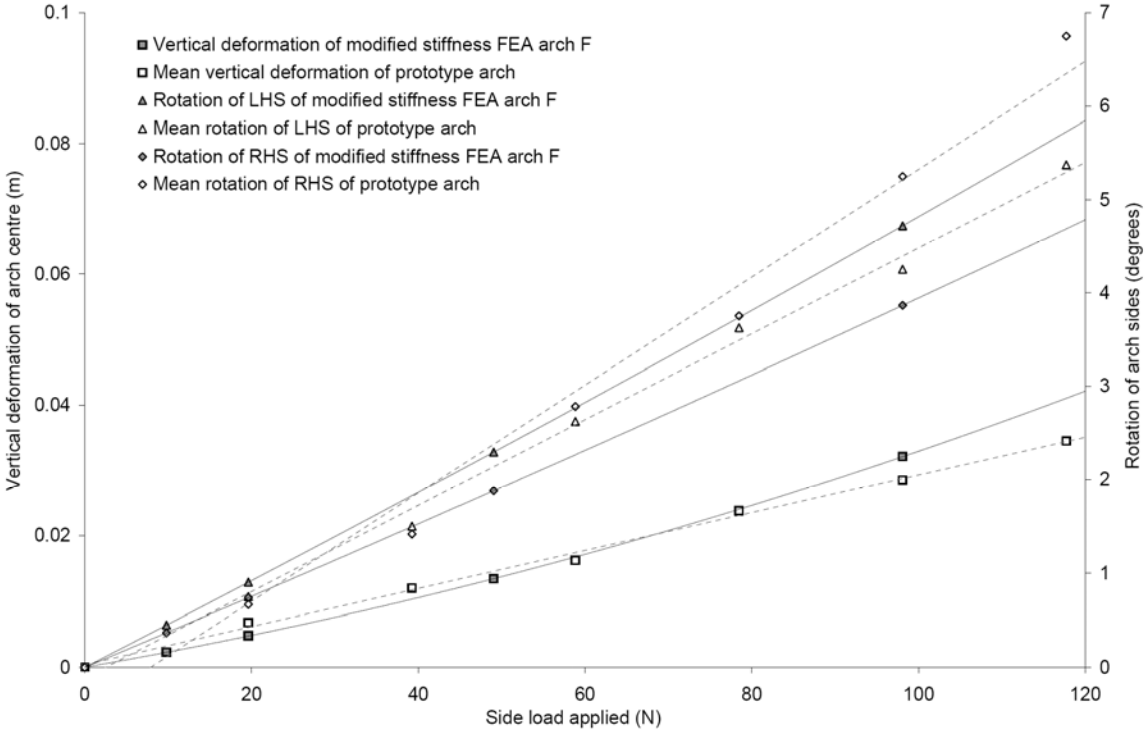

Figure 11 - Comparison of finite element model with prototype arch under side-load tests

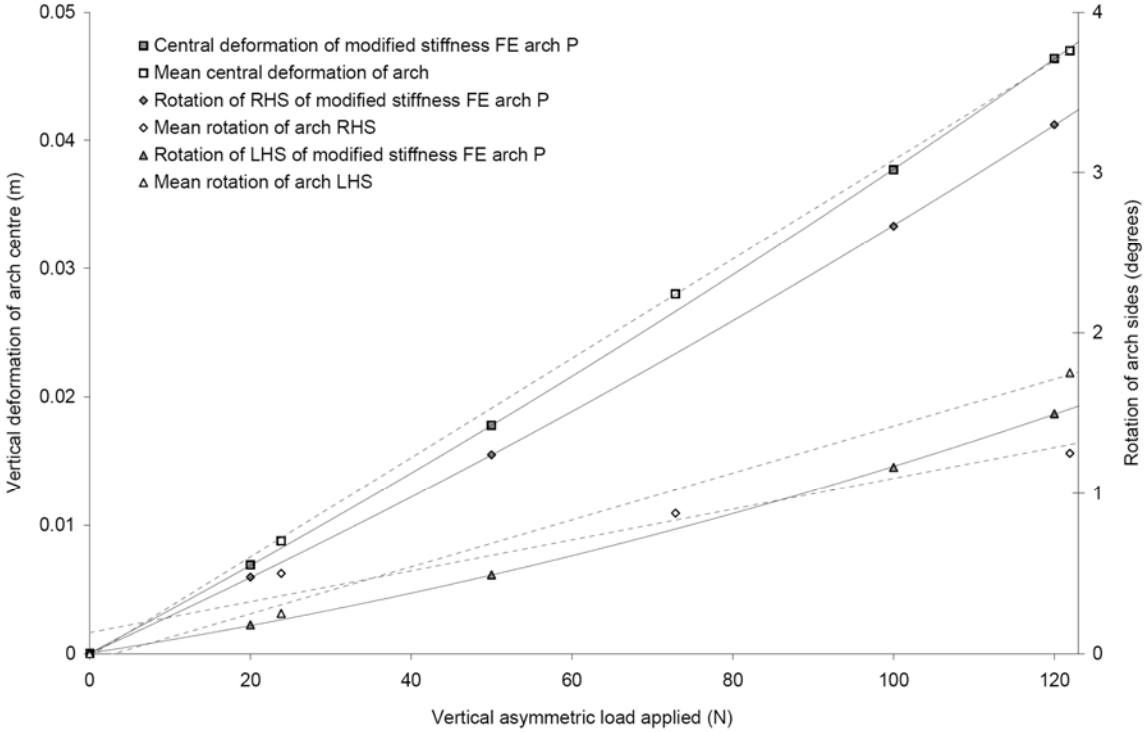

Figure 12 - Comparison of finite element model with prototype arch under asymmetric load tests

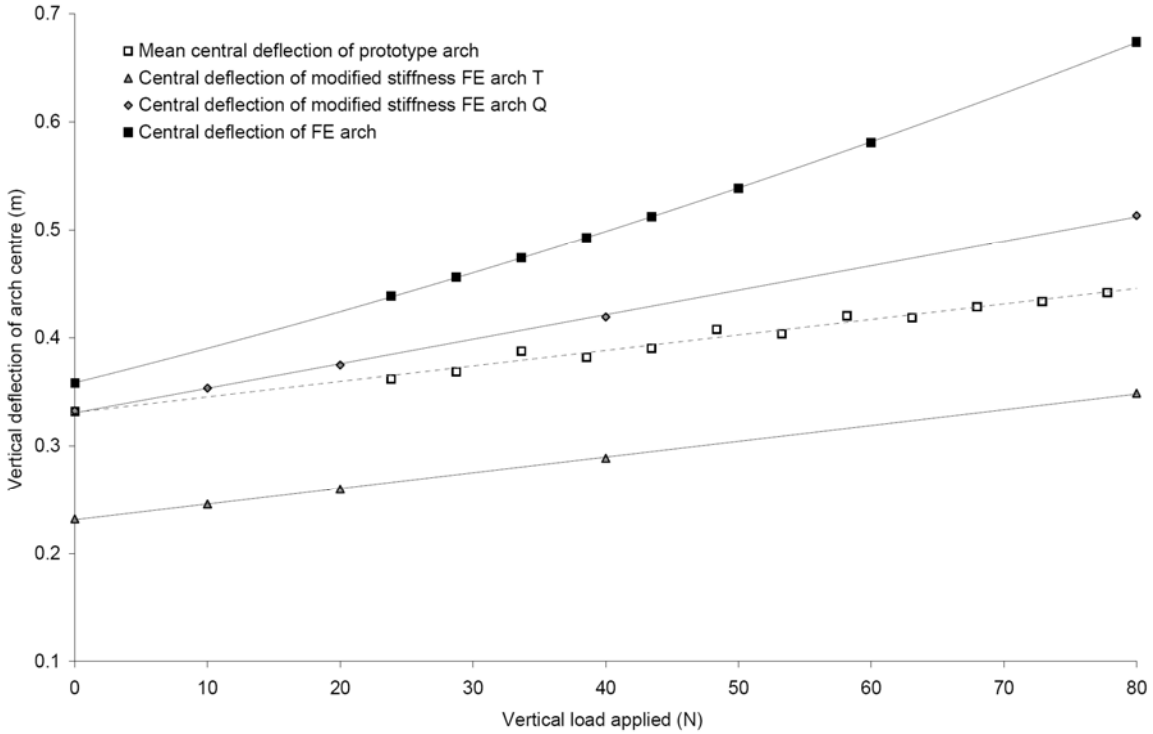

Figure 13 - Comparison of finite element models with prototype arch under braced central load tests